

# Quantifying silo flow using MRI velocimetry for testing granular flow models

Luke Fullard\*

*School of Fundamental Sciences,  
Massey University, New Zealand.*

Daniel J. Holland

*Department of Chemical and Process Engineering,  
University of Canterbury, New Zealand.*

Petrik Galvosas

*School of Chemical and Physical Sciences,  
Victoria University, New Zealand*

Clive Davies

*School of Food and Advanced Technology,  
Massey University, New Zealand.*

Pierre-Yves Lagrée, Stéphane Popinet

*Institut Jean le Rond d'Alembert,  
CNRS UMR 7190  
Sorbonne Université,  
Paris, France.*

( Dated: September 10, 2020)

In this work we present experimental results of the gravity-driven discharge of poppy seeds from 3D-printed silos. The velocity fields of the flowing poppy seeds are measured using Magnetic Resonance Imaging (MRI) velocimetry techniques. Crucially, this approach allows the velocity field to be determined throughout the flow domain, unlike visual techniques such as Particle Image Velocimetry (PIV) and related methods where only the flow at or near the wall is accessible. We perform the experiment three times; with 3D-printed silos of cone half angles  $30^\circ$  and  $50^\circ$  respectively, and then repeat the  $30^\circ$  silo experiment, but with a layer of poppy seeds glued to the silo wall to create a “rough wall” condition. In our experiments, we observe and quantify velocity fields for three well known granular flow regimes; mass flow, funnel flow, and rat-holing. The results of the experiments are compared to equivalent output of numerical simulations. In this mathematical model, the well-known  $\mu(I)$  friction law is used to define an effective granular viscosity, and the flow is solved using a standard Navier-Stokes type solver. While the results are generally encouraging, it is noted that some aspects of the model are lacking and should be improved; in particular, the rat-holing effect observed in one of the MRI experiments was not predicted by the model, nor was the exact volumetric flow rate from any of the silos. Suggestions for model improvement are discussed.

## I. BACKGROUND AND INTRODUCTION

Granular matter is well known to behave in complex and often unexpected ways. Particles in a granular assembly may act in a solid-like, liquid-like, or gas-like manner, with the transition between these phases often difficult to

---

\* L.Fullard@Massey.ac.nz

define and quantify [1]. A commonly studied granular system is gravity-driven silo discharge. In addition to being a system of great practical importance, silo flow can also display a variety of interesting flow dynamics. Depending on the design of the silo (i.e. the silo half angle, the friction between particles, the friction between the silo walls and particles, and the size and shape of the particles), the flow may be either mass-flow, funnel flow, or display rat-holing [2, 3]. In mass flow, all particles in the silo are in motion with no stagnant zones; in funnel-flow there are regions within the silo where particles flow, but there are also stagnant regions (and an interface between flowing/stagnant regions); when a silo displays rat-holing, flow only occurs in a central core approximately the size of the silo opening, with large stagnant regions surrounding this core. Rat-holing can be considered an extreme case of funnel flow, but the flow is often observed to be intermittent and transient, whereas in a general funnel flow the dynamics are much more steady. Due to the variety of flow regimes, the silo provides an excellent test of numerical models of granular dynamics.

Apart from testing numerical codes, quantifying velocity fields in the silo is of great industrial importance, for example, in the study of particle mixing and segregation as particle blends are discharged from a silo. While there have been many Discrete Element Modelling (DEM) [4–6] and continuum models [7–14] developed to study the silo, experimental measurements and validations are still required.

The vast majority of experimental characterisation of the velocity vector field in a discharging silo has been using visual imaging methods in transparent silos (both conical and planar). Techniques such as Particle Image Velocimetry (PIV) and Particle Tracking Velocimetry (PTV) have been successfully applied to measure the grain velocity *at the silo walls* [15–20]. On the contrary however, experimental measurements of velocity fields away from silo walls (i.e. in the bulk of the flow) are particularly difficult to obtain. Previous attempts to experimentally quantify 3D velocity fields in silos

have included X-ray CT [21, 22], timing tracer discharge [23], Scanning gamma ray tomography [24, 25], and single profile proton absorptiometry [26], however, all of these methods give limited velocity profile information, and usually provide averaged data, data at discrete points, or data along a line only, rather than on a plane.

Magnetic Resonance Imaging (MRI) is an alternative technique that can study flow in optically opaque systems. MRI has been applied to non-silo granular systems [27–34] to quantify parameters such as velocity fields and packing. Kawaguchi [35] observed the flow type, either mass or funnel flow, in silos using tagged MR imaging. In this approach, bands of particles are tagged at one point in time and then the positions of these tagged particles imaged after a defined delay (in this case 100 ms). The deformation of the tagged layers was observed visually. In theory this technique could be extended to estimate the velocity in a silo using further image processing techniques, but this would give only an indirect measure of the velocity fields. MRI has also been used to obtain the only reported direct, quantitative measurement of the silo velocity data on a plane away from the silo walls that we have found [36], though the range of silo flow conditions studied was limited. The first objective of the current article is to extend the work of Gentzler and Tardos [36] to obtain velocity field data for a wider range of silo flow situations. Firstly, we report on both the vertical and horizontal component of the velocity at the outlet. Secondly, we also measure particles of a large diameter ( $\approx 1\text{ mm}$ ) such that the effect of the surrounding air on the particle dynamics near the orifice is not significant [37]. Thirdly, we consider the effect of changing the hopper geometry. Finally, we consider the effect of rough-walls on the particle dynamics. These last two aspects of the experiment mean that flow is studied across the three major flow regimes observed in silos.

A second objective is to assess the applicability of the so-called  $\mu(I)$  friction law [38] for reproducing the velocity fields which we experimentally measure. Previously, the  $\mu(I)$  friction law has been used to define an effective gran-

ular viscosity for use in incompressible continuum flow models. Such an approach has been successfully applied to the granular column collapse and to some silo flows. [7, 8, 13, 39]. However, the velocity fields produced by the model have not been rigorously tested against experimental data. In particular, we examine the model applicability to reproduce the three silo flow modes, mass flow, funnel flow, and ratholing, which we observe in our experimental results.

## II. MATERIALS AND METHODS

### 1. Particle properties

In this study, poppy seeds were chosen as the granular material of interest due to their particle size, their price and availability, and the fact that they contain abundant free oil which allows a strong signal to be detected by the MRI equipment. The poppy seeds were non-spherical, and were kidney shaped, as seen in Figure 1. The poppy long diameter was approximately  $1.25 \text{ mm}$ , while the short diameter was approximately  $0.85 \text{ mm}$ . A standard sieve experiment was performed and  $\approx 93\%$  of the particles were found to be between  $710 \mu\text{m}$  and  $1180 \mu\text{m}$ , with a Sauter mean diameter [40],  $d$ , of  $951 \mu\text{m}$ .

### 2. Silo system design

The silo feeding system was designed to the specifications of the bore of the MRI apparatus in such a way that the poppy seeds were fully contained and never came in direct contact with the MRI apparatus itself. A system of perspex pipes of decreasing diameter was used to feed the poppy seeds into the test silo (the region to be imaged by the MRI) and then out of the bottom of the system. These pipes were connected using a series of push-fittings with small tolerances. Figure 2 A. displays the full system of pipes and the test silo, while B. is a close up of the silo itself. The silo was designed in

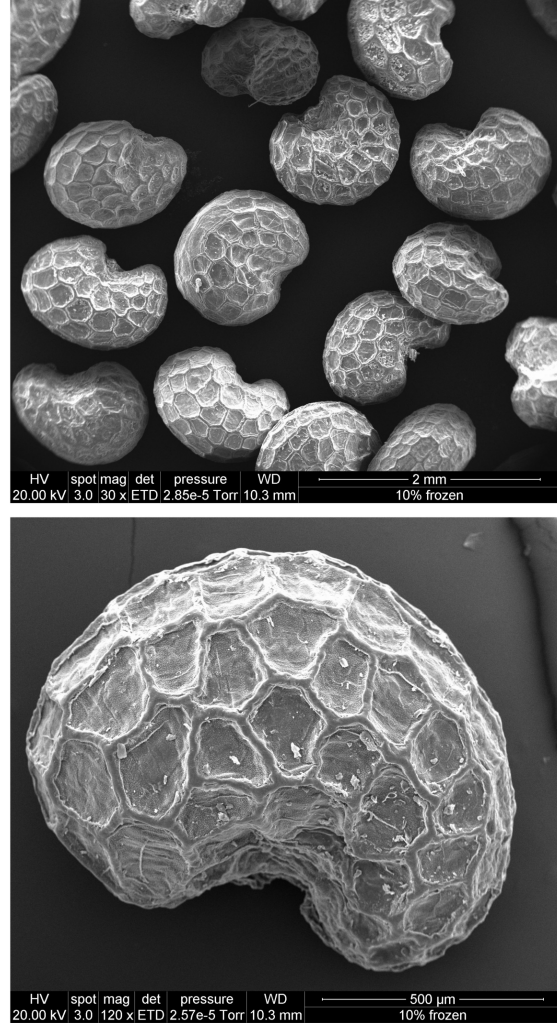


FIG. 1. Scanning Electron Microscope images of a sample of poppy seeds. It is apparent from the image that the seeds are non-spherical with a kidney shape. The surface of the seeds is also seen to be textured. A scale is included at the bottom of each image. **A.** An image of multiple poppy seeds. **B.** A close up of a single poppy seed.

a CAD program, 3D printed from ABS plastic, and the opening at the bottom of the silo,  $D_0$ , was drilled to a diameter of  $6.5 \text{ mm}$  (note that this is  $\approx 6.5$  times greater than the Sauter mean diameter,  $d$ , of the particles to avoid jamming

[18, 41]). The inner diameter of the silo,  $W$ , was  $23.5 \text{ mm}$ . Since  $D_0 > 6.5d$ ,  $W > 2.5D_0$ , and the bed height is always deeper than the silo opening diameter, the flow rate from the silo can be expected to be independent of the silo geometry. [42] The silo half angle,  $\phi$ , was changed between each experiment; the first silo had a  $30^\circ$  half angle, the second  $50^\circ$ , and the third was another  $30^\circ$  half angled silo but with rough walls. The rough walled silo was printed in two halves, then poppy seeds were glued onto the inner silo walls in a single layer, and finally, the two halves were glued together to form a full silo. We note that the diameter of the final pipe, labeled pipe 3 in Figure 2, was wider than the silo opening. This design was to avoid the well-known standpipe flow rate effect [43] which does not occur unless the pipe below the silo is full [43]. Since the silo opening diameter was smaller than the exit pipe this was not the case and the standpipe effect was avoided.

### 3. Experimental method

A Bruker Avance I Nuclear Magnetic Resonance spectrometer with a 9.4 T wide bore magnet located at Victoria University of Wellington, New Zealand was used for the experiments. A 30 mm diameter radio-frequency coil was used for excitation and detection. A three-axis shielded Micro2.5 gradient set capable of producing a maximum gradient strength of  $1.51 \text{ T m}^{-1}$  was used for imaging and flow encoding. The pipes and silo were connected together and carefully inserted into the MRI. The silo and upper two pipes were filled from above through a funnel. A bucket was placed under the system to collect the discharged particles. As the particles were discharged the system was periodically refilled from above such that the upper pipe (pipe #1) was never more than half empty. Note that the flow rate from the silo was constant and independent of fill height as is implicit in the Beverloo flow rate equation [44, 45].

The vertical (i.e. in the axial direction) and horizontal (i.e. in the radial direction) components of velocity of the poppy seeds were measured using a phase encoded velocity imaging sequence [46]. The image was obtained using a spin echo acquisition with a slice selective refocussing pulse. To enable accurate measurements of the wide range of velocities present in the system, experiments were repeated with 8 flow encoding gradients. The velocity was calculated from a linear fit to as many of these data points as possible. For the fastest flowing regions, typically only three experiments with the weakest flow encoding gradients were used, while in the slow moving regions all 8 experiments were used. The gradient encoding duration  $\delta$  was set to  $0.7 \text{ ms}$ , the observation time was  $2.5 \text{ ms}$ , and the maximum gradient strength was set to  $0.07 \text{ T m}^{-1}$  in the vertical direction and  $0.14 \text{ T m}^{-1}$  in the horizontal direction. These settings gave a maximum field of flow of approximately  $2 \text{ m s}^{-1}$  with a minimum detectable velocity of  $1 \times 10^{-3} \text{ m s}^{-1}$ ,

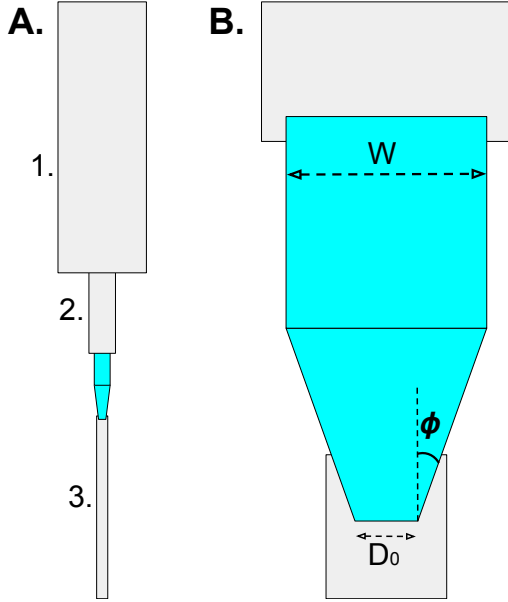


FIG. 2. A sketch of the piping and silo in the experimental set-up (not to scale).

**A.** The system is loaded from above. the seeds flow through the largest pipe #1. into the more narrow pipe #2. through the test silo section, and out through pipe #3. **B.** A close up of the test silo section.

where the minimum detectable velocity corresponds to a signal-to-noise ratio for the phase of 2. Images were acquired at a spatial resolution of  $0.45 \text{ mm}$  in the horizontal direction and  $1.18 \text{ mm}$  in the vertical direction with a slice thickness of  $1 \text{ mm}$ . The total acquisition time for the images was approximately 50 minutes. Flow-encoded NMR images can acquire a phase arising from the imaging gradients themselves. It is common practice to correct this phase by acquiring measurements on a static sample. Here images of a static bed were also acquired. The phase change for these was negligible, thus no correction was required.

Three MRI experiments were performed, one with a silo of  $30^\circ$  half angle, one with a silo of  $50^\circ$  half angle, and finally with another silo of  $30^\circ$  half angle, but with rough walls (with particles glued on the silo walls).

#### 4. Numerical model

One goal of this work is to model the silo using a continuum model of granular flow. Recently, the  $\mu(I)$  law for the friction of granular materials has been used to define an effective viscosity in granular flow simulations. This viscosity was successfully implemented into an incompressible Navier-Stokes solver (Gerris Flow Solver [47]) to model dense granular flow in a variety of situations [7, 8, 13, 39]. For our situation, an axisymmetric domain was used so that our 3D silo could be modelled in 2D. The governing equations of incompressible flow were solved in Gerris;

$$\nabla \cdot \mathbf{u} = 0, \quad (1)$$

$$\rho \left( \frac{\partial \mathbf{u}}{\partial t} + \mathbf{u} \cdot \nabla \mathbf{u} \right) = -\nabla p + \nabla \cdot (2\eta \mathbf{D}) + \rho \mathbf{g} \quad (2)$$

In the above continuity and momentum equations,  $\mathbf{u}$  is the velocity vector,  $\rho$  the flowing (bulk) density,  $p$  the local isotropic pressure,  $\eta$  the effective (or apparent) granular viscosity, and  $\mathbf{D}$  the rate of strain tensor. The effective viscosity is defined as

$$\eta_{eff} = \frac{\mu(I)p}{D_2}, \quad (3)$$

but in practice a regularised effective viscosity was used to avoid infinite values when the fluid is experiencing small shear;

$$\eta = \min \left( \frac{\mu(I)p}{D_2}, \eta_{max} \right). \quad (4)$$

Here,  $D_2 = \sqrt{\frac{1}{2} D_{ij} D_{ij}}$  is the second invariant of the strain rate tensor, where  $D_{ij} = \frac{\partial u_i}{\partial x_j} + \frac{\partial u_j}{\partial x_i}$ , and  $\mu(I)$  is the granular friction law;

$$\mu(I) = \mu_1 + \frac{\mu_2 - \mu_1}{I_0/I + 1}, \quad (5)$$

with  $\mu_1$ ,  $\mu_2$ , and  $I_0$  parameters. The variable  $I$  is the granular inertial number and is defined as

$$I = \frac{d D_2 \sqrt{\rho_p}}{\sqrt{p}}, \quad (6)$$

where  $d$  is the particle diameter and  $\rho_p$  is the solid particle density.

In our axisymmetric numerical model we apply no-slip conditions on both of the velocity components at the silo walls, a symmetry condition along the axis of symmetry, homogeneous Neumann velocity boundary conditions (for each velocity component) at the top and bottom of the silo, and we set  $p = 0$  at the top and bottom of the silo. Note that other boundary conditions could be used at the silo wall (for example, to allow slip at the silo wall [48, 49]), but the effect of more complex boundary conditions is left for future work. For the  $30^\circ$  silo with rough walls, the simulation domain was reduced by a particle diameter in size to account for the reduced dimensions due to the layer of particles glued to the silo walls, but the silo opening was kept at  $6.5 \text{ mm}$ . No other change to the boundary conditions was made.

Parameters used in our simulation are listed in table I. The first friction parameter,  $\mu_1$ , was chosen based on measurements of the angle of repose of the poppy seeds which was found to be approximately  $31^\circ$ , hence,  $\mu_1 = \tan 31 = 0.6$ . The upper limit on the friction angle, defined by parameter  $\tan^{-1}(\mu_2)$ , was expected to be

around  $60^\circ$  since our MRI experimental results for the velocity in the  $30^\circ$  silo (to be presented in Figure 3) showed small slow/stagnant regions at the transition from the conical to cylindrical section. We also noted that larger values of  $I_0$  kept the incompressible  $\mu(I)$  model in the well-posed regime for a wider range of inertial numbers than for low values of  $I_0$  [50]. For this reason, various values of  $\tan^{-1}(\mu_2) \approx 60^\circ$  and  $I_0$  between 0.05 and 1 were tested. It was found that the parameters  $\mu_2 = 1.7$  and  $I_0 = 0.5$  gave a good match to experimental data (to be discussed), gave a wide range of well-posed inertial number values, and, importantly, were physically realistic.

TABLE I: Parameters used in the numerical model.

Name	Symbol	Unit	Value
Bulk density	$\rho$	$kg/m^3$	600
Particle density	$\rho_p$	$kg/m^3$	1000
Particle diameter	$d$	$mm$	0.951
Friction coefficient #1	$\mu_1$	-	0.6
Friction coefficient #2	$\mu_2$	-	1.7
Reference inertial number	$I_0$	-	0.5

### III. RESULTS

#### 1. MRI Experimental Results

The results of the phase encoded velocity imaging sequence experiment were converted into a Matlab data file and plotted as a contour map. In Figure 3 the logarithm of the vertical component of velocity is plotted for each of the three silos, where  $\mathbf{u} = (u, v)$  is the velocity vector with  $u, v$  the horizontal and vertical velocity components respectively. The logarithm of the magnitude of the horizontal component of velocity ( $u$ ) is shown in Figure 4. The lighter (yellow) regions are zones of rapid flow, while the darker (purple/blue) regions indicate slow or stagnant flow. Horizontal velocity measurements were not available for the  $30^\circ$  silo with rough walls because the magnitude of the horizontal component of velocity was very small and

was of the same order as the noise in the experiment.

The most immediate observation from Figure 3 is that for each silo we have a different flow regime. In the  $30^\circ$  silo we observe mass flow. The particles in the silo at every location are in motion, with a possible small exception at the transition from the cone to the cylindrical section. In the  $50^\circ$  silo we observe funnel flow. There is a region of flow in the center of the silo and this region of flowing material widens as we move further up into the silo. There is a clear stagnant region of flow that surrounds the flowing particles. This stagnant region shrinks as we transition higher into the silo. In the  $30^\circ$  silo with rough walls (i.e. with a layer of poppy seeds glued to the wall) we observe the rat-holing effect. There is a fast core (roughly the diameter of the silo opening) of flowing particles surrounded by a region of stagnant material. The size of this stagnant zone does not perceptibly change as we transition higher into the silo. It is also apparent that the velocity field in the flowing zone remains continuous as we move higher in the silo, past the transition from the conical to cylindrical section (i.e. we do not observe velocity discontinuities or shocks). This is in contrast to predictions from Mohr-Coulomb plasticity based models [2, 51].

In order to assess the appropriateness of the incompressible assumption in our numerical model, we quantify the volumetric flow rate as a function of height above the silo opening. For each MRI experiment we use the vertical component of velocity ( $v$ ) to calculate the volumetric flow rate;

$$Q(z) = 2\pi \int_{r(z)=0}^{r(z)=R(z)} v r dr, \quad (7)$$

where  $r(z)$  is the radial coordinate from the axis of the silo, and  $R(z)$  is the radius of the silo at height  $z$  above the opening. The resulting flow rates for each experiment are plotted in Figure 5.

It is apparent from the figure that the volumetric flow rate is approximately constant throughout the silo in the  $30^\circ$  silo, but this is not so for the  $50^\circ$  and  $30^\circ$  silo with roughened

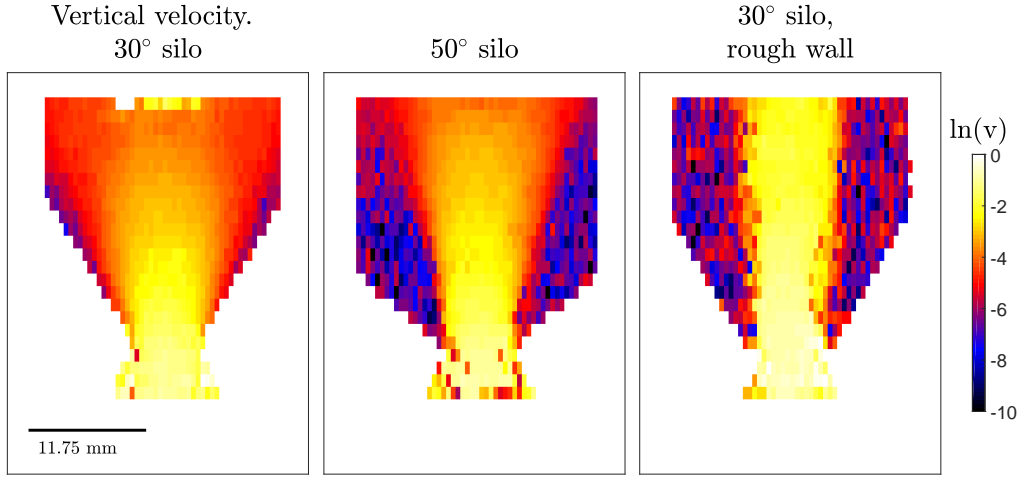


FIG. 3. The log of the magnitude of the vertical component of velocity ( $v$ ) is plotted for each of the three silos. Mass flow is observed in the 30° silo, funnel flow in the 50°, and rat-holing in the 30° silo with rough walls (with particles glued to the silo wall). Yellow regions indicate rapid flow, while purple/blue areas indicate slow to stagnant zones.

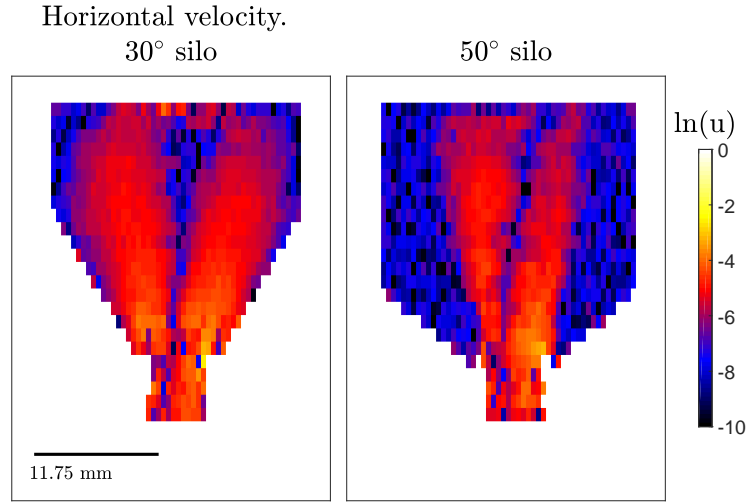


FIG. 4. The log of the magnitude of the horizontal component of velocity ( $u$ ) for the 30° and 50° silos.

414 walls. In these two non-constant flow rate cases, 420  
415 the volumetric flow rate  $Q(z)$  is seen to be  $\approx 2 \times$  421  
416 higher near the opening than it is in the bulk of 422  
417 the silo. This variation in flow rate could arise 423  
418 either from a measurement error or a dilation 424  
419 of the flow at the outlet. The signal intensity 425

at the outlet in all three images is less than half  
that in the bulk, which would be consistent with  
a dilation of the flow at the outlet. However,  
in these measurements there is also significant  
attenuation of the signal due to the motion of  
the particles, so the images are not quantitative

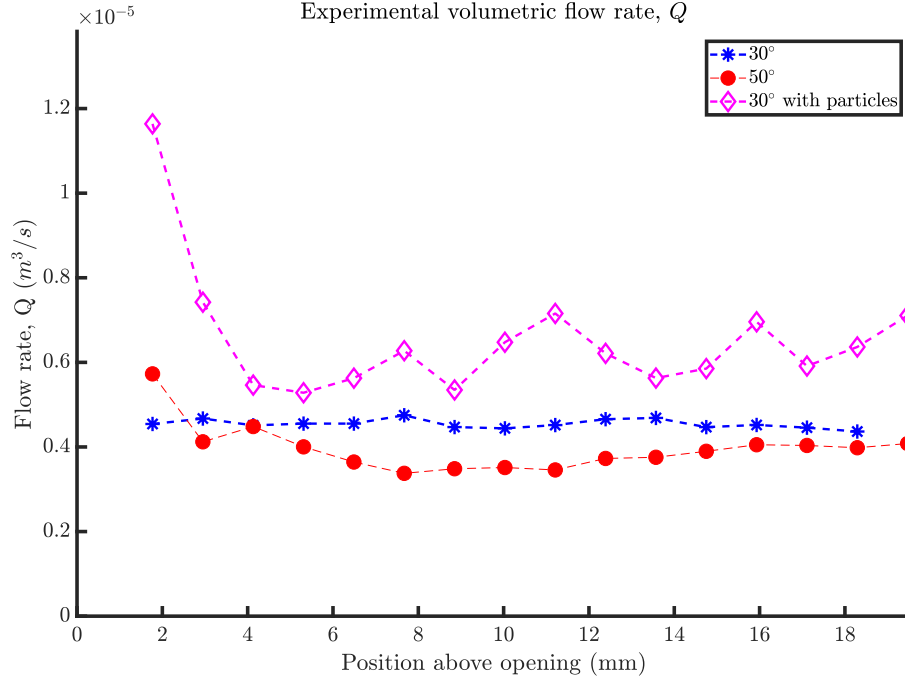


FIG. 5. The volumetric flow rate,  $Q(z)$ , for each of the three silo experiments as a function of height above the silo opening.

in solid fraction. Therefore it is important to consider the errors that arise in measurement of velocity. MRI measurements of the velocity are prone to error in regions of high velocity but this error will tend to cause an underestimation of the velocity as faster moving particles are more heavily attenuated than slower moving particles. The flow rate is seen to increase towards the outlet, hence, it is unlikely that a velocity measurement error could explain the observed flow rate variation. Therefore, it is concluded that, for the funnel flow and rat-holing silos, there is significant dilation of the flow near the opening, and the assumption of incompressibility is likely to be erroneous, at least near the silo opening. In a similar system, a wedge shaped hopper, a significant reduction in bulk density has been observed [52]. As a point of context, in the numerical model the incompressibility condition is enforced (up to a tolerance) and it was found that the change in the volumetric flow rate was less than 1% throughout the silo. Here we assume that the use of an incompressible flow model has only a small effect on the predicted velocity fields, since in the bulk of the silo the flow rate is relatively constant, changing only near the silo opening. However, the dilation near the opening will change the predicted flow rate values. Given this result and model assumption, when comparing experimental and numerical results with an incompressible flow assumption, the velocity should be adjusted to account for the change in volumetric flow rate. In practice this is achieved by normalising the velocity by the volumetric flow rate at each local height above the silo opening. Furthermore, we quantified the mass flow rate,  $\dot{m}$ , from each of the silos by measuring the mass ejected from the system in a given time. For the 30° silo we found  $\dot{m}_{30} = 2.11 \pm 0.07$  g/s, for the 50° silo,  $\dot{m}_{50} = 1.74 \pm 0.09$  g/s, and for the 30° silo with particles on the wall,



468  $\dot{m}_{30}^p = 2.2 \pm 0.1 \text{ g/s}$ . The reduction of the 512  
 469 mass flow rate between the  $30^\circ$  and  $50^\circ$  silos 513  
 470 is compared with corrections made to the Bev- 514  
 471 erloo flow rate to account for hopper half angle 515  
 472 [53]. Assuming that the Beverloo parameters 516  
 473 and bulk density is equal between the two silos 517  
 474 of differing half angles, the ratio of the two flow 518  
 475 rates is given as  $M = \frac{f(50^\circ)}{f(30^\circ)}$ , where the func- 519  
 476 tion  $f(\alpha) = \sqrt{\frac{1 - \cos \alpha}{2 \sin^3 \alpha}}$ . The theoretical ratio  $M$  520  
 477 is calculated as 0.86, while the experimental ra- 522  
 478 tio in our system,  $\frac{\dot{m}_{50}}{\dot{m}_{30}}$  is found to be  $0.82 \pm 0.05$ , 523  
 479 in good agreement with the theoretical value. 524

## 480 2. Numerical Model Results: $30^\circ$ silo 527

481 To directly compare the  $\mu(I)$  numerical re- 529  
 482 sults to the MRI experimental results a results 530  
 483 file was imported from Gerris into Matlab which 531  
 484 contained vertical and horizontal components of 532  
 485 velocity. This data was interpolated onto five 533  
 486 horizontal lines which correspond to the loca- 534  
 487 tions of measurements taken in the MRI exper-  
 488 iments. Thus, the horizontal and vertical com-  
 489 ponents of velocity predicted in the model could 535  
 490 be directly compared to the experimental data.

491 As previously mentioned, the volumetric flow 536  
 492 rate in the silo experiments was not a constant 537  
 493 near the opening of the silo. Therefore, both 538  
 494 the experimentally measured and numerically 539  
 495 predicted velocity data were normalised by the 540  
 496 volumetric flow rate before being compared. At 541  
 497 each height above the silo opening,  $z$ , the local 542  
 498 volumetric flow rate is calculated using Equa- 543  
 499 tion 7. The velocity components are then mul- 544  
 500 tiplied by the particle diameter squared and di- 545  
 501 vided by the local volumetric flow rate to obtain 546  
 502 the normalised velocity,  $\tilde{\mathbf{u}}$ , where  $\tilde{\mathbf{u}} = \mathbf{u}d^2/Q$ . 547

503 The comparison of the vertical velocity pro- 548  
 504 file taken at five heights above the opening for 549  
 505 the  $30^\circ$  silo with smooth walls (i.e. no parti- 550  
 506 cles attached to the wall) is shown in Figure 6, 551  
 507 while the horizontal velocity profile is shown in 552  
 508 Figure 7. The distance from the silo opening 553  
 509 to the silo transition (the point where the cone 554  
 510 becomes a cylinder) is  $\approx 14.7 \text{ mm}$ , hence four 555  
 511 of the comparison lines are in the converging 556

conical section of the silo, while one is in the cylindrical section.

It is apparent that the match between the experimentally derived and numerically predicted normalised velocity is good, particularly for the vertical velocity. The normalised velocity predicted by the model has approximately the same maximum and also approximately the same curvature and shape as the MRI experimental measurements. However, the absolute velocity predicted by the model does not match the experiment due to the discrepancy in the volumetric flow rate between the two. There is more noise in the horizontal measurements, and the prediction of normalised horizontal velocity is slightly worse near the silo opening, but overall the agreement is satisfying.

As a further test, in Figure 8 we plot the normalised vertical component of velocity along the axial centerline of the silo and compare the experiment to the model. It is apparent that the model prediction is in very good agreement with the experimental results.

## 557 3. Numerical Model Results: $50^\circ$ silo 558

In Section III 2, the comparison of numerical and experimental velocity fields for the  $30^\circ$  silo with smooth walls, there were no stagnant regions in the flow domain. The transition from flowing to stationary is difficult to capture with simple incompressible Navier-Stokes based models. Figures 9 and 10 show the normalised vertical and horizontal velocity measurements and predictions in the  $50^\circ$  silo. In this silo the distance from the silo opening to the transition point is  $\approx 7.1 \text{ mm}$ , hence in this case two of our velocity contours are in the conical section, while the remaining three are in the cylindrical section.

Remarkably, the match between experimental and numerical model results is quite good. Despite the observed transition from a flowing to a stagnant state in the silo domain, the granular viscosity model is able to capture the (normalised) maximum velocity, the curvature and shape of the velocity contours, and the approx-

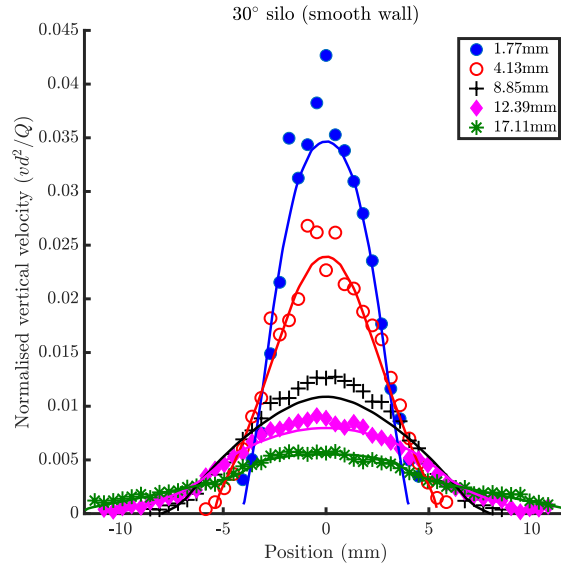


FIG. 6. The vertical velocity MRI measurements (solid circles) compared with those predicted by the numerical model (lines) for the 30° silo.

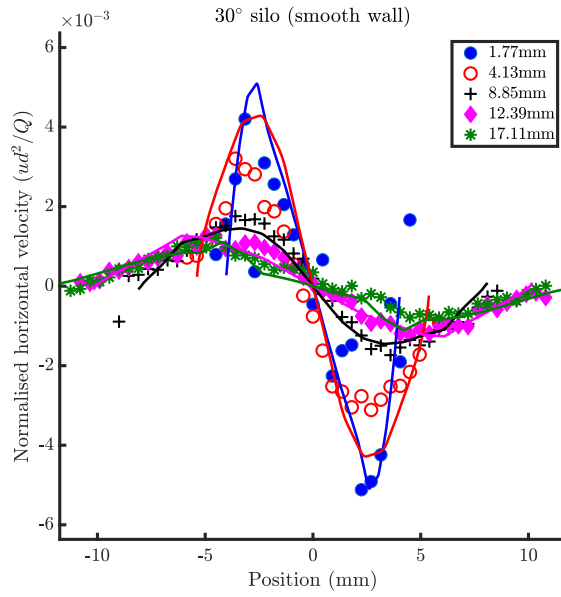


FIG. 7. The horizontal velocity MRI measurements (solid circles) compared with those predicted by the numerical model (lines) for the 30° silo, at the same locations as in the vertical velocity figure.

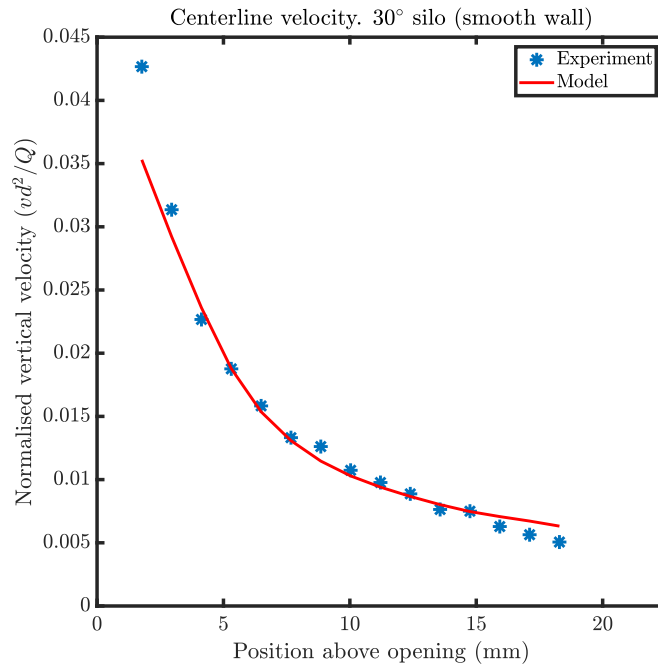


FIG. 8. A comparison of the normalised vertical velocity measured along the axial centerline of the silo compared with that predicted by the model for the 30° silo.

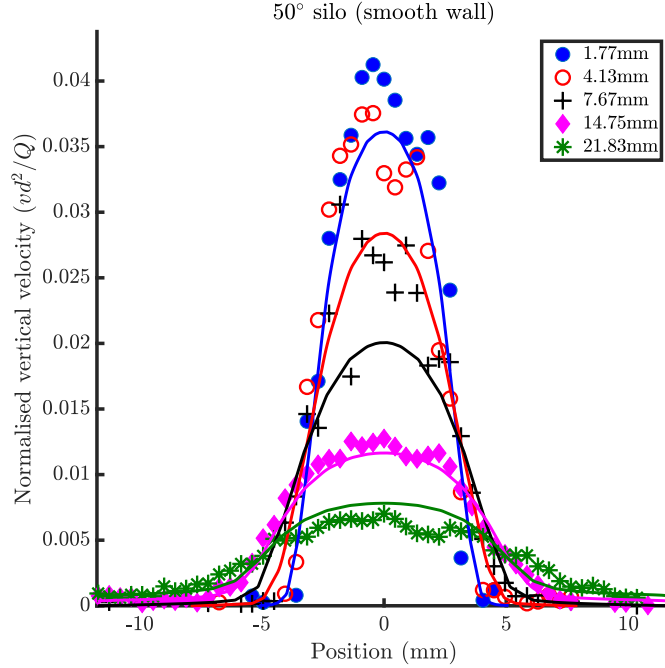


FIG. 9. The vertical velocity MRI measurements (solid circles) compared with those predicted by the numerical model (lines) for the 50° silo.

imate location of the solid/flowing boundary.

Figure 11 compares the model to experimen-  
tal normalised vertical velocity along the axial  
centerline of the 50° silo. In this case the ex-  
perimentally measured velocity contains more  
noise than in the 30° case, but it is apparent  
that the model and experiment are of similar  
and follow a somewhat similar decrease. How-  
ever, the comparison is not quite as good as in  
the 30° case.

#### 4. Numerical Model Results: 30° silo with rough walls

The most challenging flow regime to replicate  
is the rat-holing behaviour observed in the 30°  
silo with roughened walls. In this case the ob-  
served magnitudes of horizontal velocity were  
too small to quantify since they were impercep-  
tible from the experimental noise. Hence, the

comparison of experimental to numerical pre-  
dictions was only possible for the vertical ve-  
locity component. Figure 12 displays the nor-  
malised vertical velocity profile at five heights  
above the silo opening, while Fig. 13 is the  
normalised vertical velocity measured and pre-  
dicted along the axial centerline of the silo.

It is apparent that the  $\mu(I)$  model predictions  
completely fail to replicate the measured veloc-  
ity, particularly far from the silo opening. In  
the case of rat-holing flow, the  $\mu(I)$  model is  
unable to capture the observed dynamics.

#### 5. Numerical Model: Sensitivity analysis and flow rates

In order to further compare the experimental  
and numerical velocity predictions we compare  
predicted flow rates between the numerical and  
experimental results, and perform a sensitivity

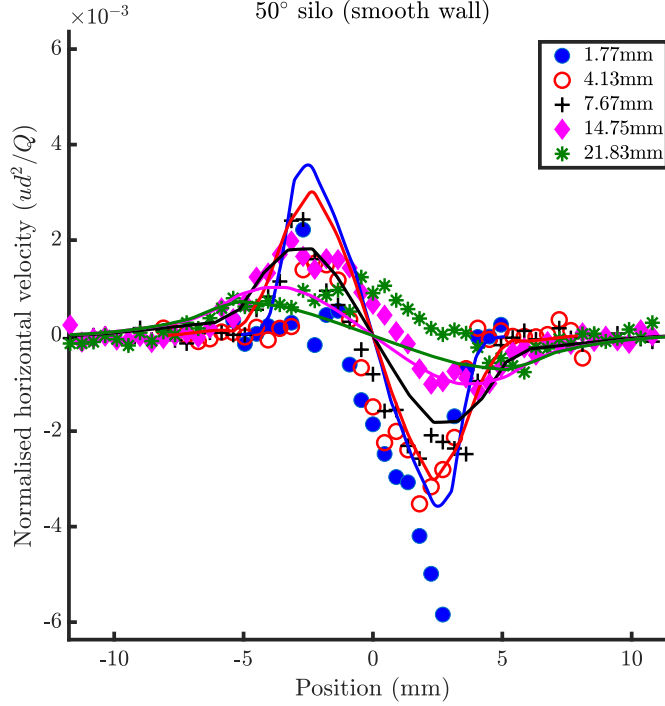


FIG. 10. The horizontal velocity MRI measurements (solid circles) compared with those predicted by the numerical model (lines) for the  $50^\circ$  silo. at the same locations as in the vertical velocity figure.

analysis on the numerical model parameters.

To quantify the “goodness of fit” of the numerical predictions of velocity to the experimentally measured ones we perform linear least-squares regression on the normalised vertical velocity data:  $\tilde{v}_{num} = b\tilde{v}_{exp}$  (i.e. we force the regression to pass through the origin). In the case of a perfect fit between the numerical and experimental data, the slope of the line,  $b$ , would be unity. The normalised vertical velocity data at five heights above the silo opening (the same heights as used in Figures 6, 9) are combined and the regression is performed on the entirety of this data at once. To test the sensitivity of the model predictions to model parameters this process was repeated 65 times for different values of  $I_0$  and  $\mu_2$ . This analysis was performed for both the  $30^\circ$  and  $50^\circ$  silos, resulting in 130 numerical simulations. In each simulation the value of  $\mu_1$  was kept constant at 0.6,

while the ranges of the other two parameters were  $0.05 < I_0 < 1$ , and  $0.9 < \mu_2 < 2.1$ . In Figure 14 the slopes resulting from the linear least-squares regression analysis are contoured for the  $30^\circ$  (left) and  $50^\circ$  (right) silo flows respectively. The solid red dot in the contour plots indicates the values of the parameters used in the current work to produce Figures 6 - 13. The fine red line in the left plot is the contour of slope = 1 which represents a perfect fit of the numerical prediction of normalised vertical velocity to its experimental measurement. In general, the  $30^\circ$  silo numerical simulation was better fit for lower  $I_0$  and larger  $\mu_2 - \mu_1$  values, while the  $50^\circ$  simulation had the opposite behaviour. The  $30^\circ$  simulation was always better fit to the experimental data than the  $50^\circ$  one, with reported slopes in the range 0.86 to 1.03 (by comparison, the  $50^\circ$  silo slopes were in the range 0.65 to 0.89). For the parameters used in the main

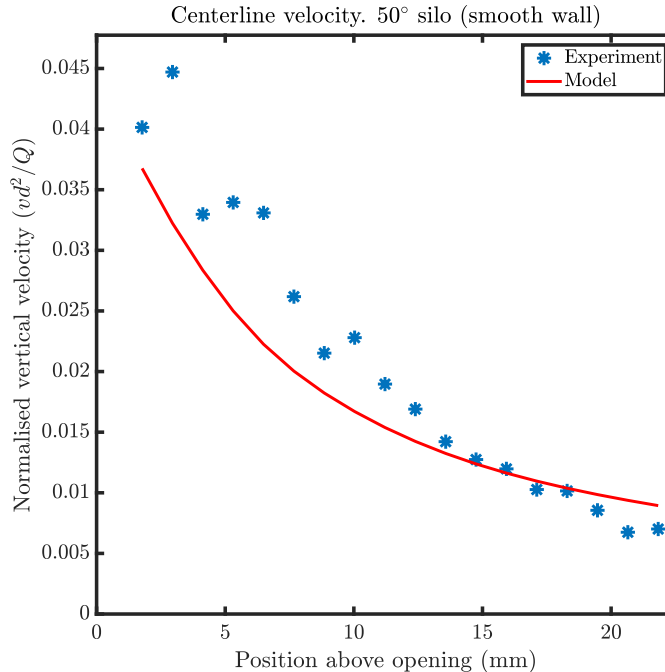


FIG. 11. A comparison of the normalised vertical velocity measured along the axial centerline of the silo compared with that predicted by the model for the 50° silo.

text (see Table I) the least squares slopes were 0.94 for the 30° silo, and 0.84 for the 50° one. Overall, the choice of the parameters  $I_0 = 0.5$  and  $\mu_2 = 1.7$  used in this work is shown to be a good balance between accuracy for both the 30° and 50° silos.

Table II presents, for each of the three silos, the experimentally derived mass and volumetric flow rates, the numerically predicted volumetric flow rate, and an approximate solids volume fraction in the bulk of the silo. The solids volume fraction in the bulk was approximated by taking the ratio of the experimental mass and volumetric flow rates (in the bulk of the silo), then dividing by the particle density ( $\approx 1000 \text{ kg/m}^3$ ). The predicted flowing solids fraction in the bulk of the 30° and 50° silos is remarkably similar (0.46 and 0.47 respectively). However, the 30° silo with particles glued to the wall shows a significantly lower solids volume fraction of 0.36. As previously noted, the numerical

model was of incompressible type, hence was not able to accurately predict the correct flow rate. In the table the predicted volumetric flow rate in the 30° silo simulation was a factor of  $\approx 4.5$  smaller than the experimentally observed one. The volumetric flow rate predicted in the 50° silo simulation was a lot closer to the experimentally observed rate, but we caution against interpreting this as a validation of the model. During the sensitivity analysis the predicted flow rate varied by a factor of ten over the ranges of the parameters tested, which indicates that it is sensitive to model parameter choice.

#### IV. DISCUSSION AND CONCLUSIONS

In this work we have presented results of experimental and numerical investigation of silo flow in three flow regimes; mass flow, funnel

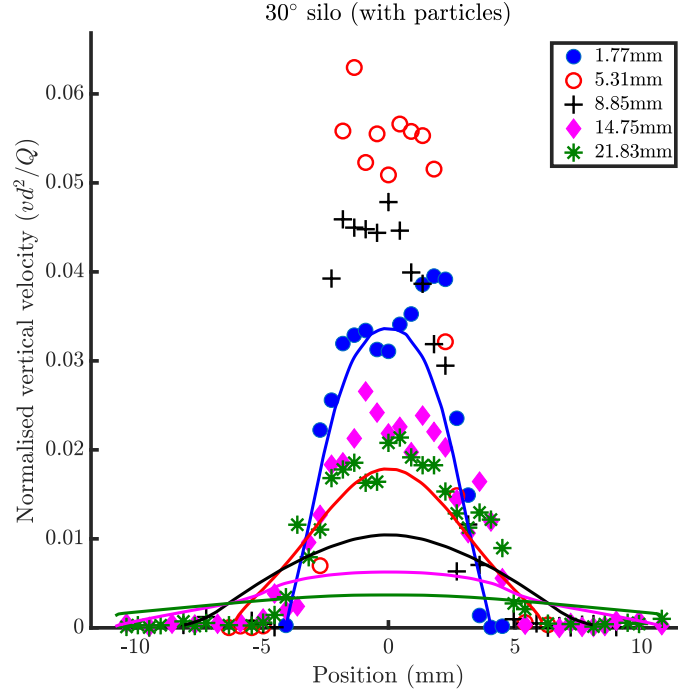


FIG. 12. The vertical velocity MRI measurements (solid circles) compared with those predicted by the numerical model (lines) for the 30° silo with roughened walls.

TABLE II: The experimentally derived and numerically predicted flow rates in the tested silos.

	$\dot{m}$ (g/s)	$Q_{exp}$ (bulk, $cm^3/s$ )	$Q_{num}$ ( $cm^3/s$ )	$\sim\phi_{exp} = (\dot{m}/Q_{exp})/\rho_p$
30°	$2.11 \pm 0.07$	$4.54 \pm 0.05$	0.97	$0.47 \pm 0.02$
50°	$1.74 \pm 0.09$	$3.8 \pm 0.1$	4.2	$0.46 \pm 0.04$
30° (with particles)	$2.2 \pm 0.1$	$6.1 \pm 0.3$	0.81	$0.36 \pm 0.04$

673 flow, and rat-holing. Using MRI velocimetry we687  
 674 measured both the horizontal and vertical com-688  
 675 ponents of velocity throughout the three test689  
 676 silos, including the transition from the converg-690  
 677 ing conical to the cylindrical section. We found691  
 678 that the 30° silo produced a mass flow, the 50°692  
 679 silo produced a funnel flow, and the 30° silo with693  
 680 rough walls produced a rat-holing flow. We also694  
 681 presented results of a numerical model which695  
 682 used the  $\mu(I)$  friction law to define an effec-696  
 683 tive granular viscosity for dense granular flow.697  
 684 This viscosity was used to simulate the silo flows698  
 685 by means of incompressible computational fluid699  
 686 dynamics.700

It was observed that the apparent volumetric flow rate in the MRI experiments was constant in the 30° silo, but was a function of height above the silo opening for the other two; the flow rate was large near the silo opening but then rapidly fell to a near constant higher in the silo. The flow rate near the opening was roughly  $2\times$  that of the bulk, indicating that there is significant dilation of the flow near the silo exit opening in the 50° and 30° with rough wall cases. This is in contrast to the numerical model which enforced incompressibility of the flow. Recent studies have quantified the effect of solids fraction value at the silo opening on the

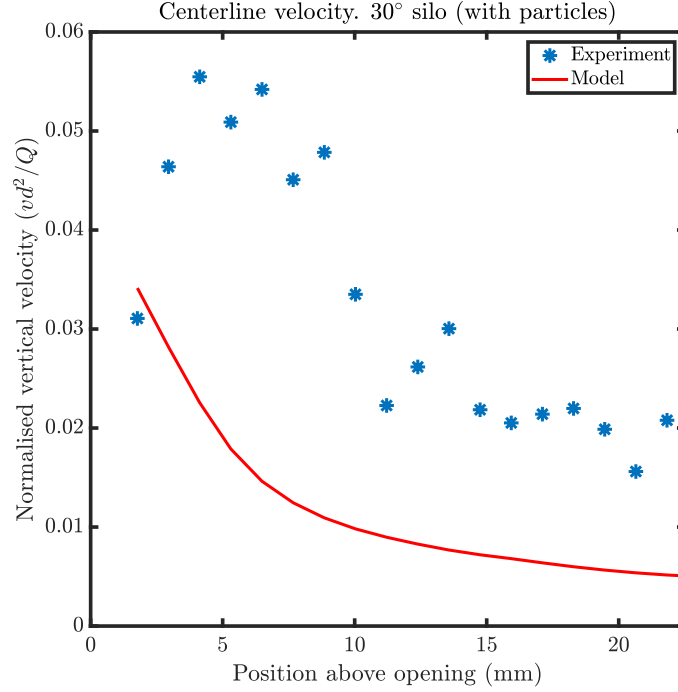


FIG. 13. A comparison of the normalised vertical velocity measured along the axial centerline of the silo compared with that predicted by the model for the 30° silo with roughened walls.

flow rate from the silo [54], and reported that solids fraction in the near opening region could be as low as half that in the bulk of the silo. We conclude that to fully capture the experimental measurement of the flow rate (and hence, the exact values of velocity) numerical models will likely need to include dilation effects, particularly for funnel and rat-holing flows. The effect of dilation for the mass flow silo appeared negligible, but may be important to accurately predict the volumetric flow rate from the silo.

To allow comparison between our experimental and numerical results, the velocity components of each were normalised by the local value of volumetric flow rate (i.e. the flow rate at height  $z$  above the silo opening). The resulting velocity fields derived from the 30° silo simulation showed excellent agreement with the experimental data. Plots of the vertical and horizontal velocity at a series of heights above the

opening showed that both the shape and (normalised) maximum of the velocity contours were well matched, as was the vertical velocity component measured along the center-line of the silo. The comparison in the 50° silo (which operated in the funnel flow regime in the MRI experiment) were surprisingly impressive, with very good agreement between experimental and numerical results. This suggests that for appropriate values of fitting parameters the  $\mu(I)$  friction law can be used to define an effective granular viscosity for granular dynamics, even in the case where there are transitions from static to flowing regions in the domain of study.

However, for the 30° silo with roughened walls (which displayed rat-holing in the MRI experiment), the simulation results were poorly matched to the experimental data. The grain dynamics in this silo are very complicated and hard to capture with numerical models. Rat-



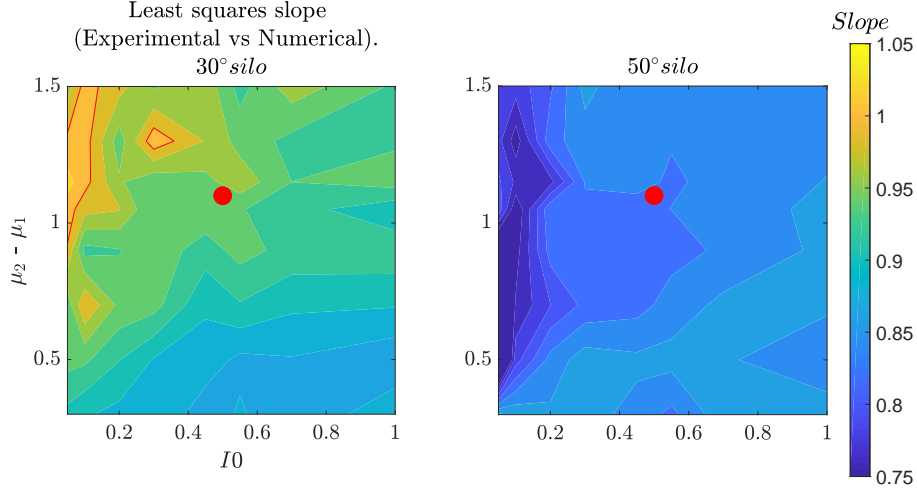


FIG. 14. Sensitivity analysis of the numerical model to parameters  $I_0$  and  $\mu_2 - \mu_1$ . The contour plots display the value of the slope found by performing a least-squares linear regression between the experimental and numerical normalised vertical velocity data. The left graph is the analysis for the  $30^\circ$  silo and the right for the  $50^\circ$  one. The red dot in the plots indicated the value of the parameters used in the current work, while the fine red line in the left plot is the contour of slope = 1 (indicating a perfect fit of the numerical to experimental data).

holing flow in a silo is often avoided by smooth-  
ing the silo walls (thus, changing the stress dis-  
tribution in the silo) and/or increasing the size  
of the silo opening. It is a challenge for simple  
incompressible continuum visco-plastic models  
of granular flow to capture these “finite particle  
size” effects. Further work is needed, includ-  
ing adding the effect of compressibility, to fully  
capture the observed dynamics in this situation.

It is clear that the  $\mu(I)$  model performs ad-  
mirably in a silo in the mass and funnel flow  
regimes for the parameter values chosen, but  
further model development is needed to fully  
capture the observed phenomena in rat-holing  
flow, and to accurately predict the flow rate  
from the silo. Adding in a degree of compress-  
ibility into the model and/or accounting for  
granular non-locality and finite size effects may  
improve flow rate predictions in the silo and  
may help to capture more accurately flowing to  
stagnant phase transitions and potentially the  
rat-holing phenomenon [55]. Testing these hy-  
potheses is currently being pursued by the au-

thors. Additionally, the  $\mu(I)$  friction law was  
discovered using experimental data from rela-  
tively low friction spherical particles [56, 57]. It  
is unclear if the  $\mu(I)$  model is the correct fric-  
tion law to use for natural particles such as the  
poppy seeds used in this work. Furthermore,  
particle shape has been shown to be an impor-  
tant factor in the behaviour of general granular  
systems [58, 59], and silo systems specifically  
[60, 61]. Using SEM imaging we found that  
our poppy seeds were kidney bean shaped, and  
not spherical. Such an effect could be impor-  
tant to include in a numerical model of granular  
flow, although the factor does not seem critical,  
since we obtained very good agreement between  
experimental and numerical results for the  $30^\circ$   
and  $50^\circ$  silos. The  $\mu(I)$  parameters in the nu-  
merical model were our “best guess”. The first  
friction coefficient,  $\mu_1$ , was taken as the angle  
of repose of the poppy seeds, however,  $\mu_2$  and  
 $I_0$  were chosen to be physically realistic and to  
try to reduce the ill-posed regions for the  $\mu(I)$   
model [50]. To check the dependence of model

results on the  $I_0$  and  $\mu_2$  parameters a sensitivity analysis was performed. It was found that the accuracy of the model was retained over a wide range of parameter values, and that our choice of  $I_0$  and  $\mu_2$  was a good balance of accuracy for both the 30° and 50° silos. To reduce model degrees of freedom these parameters should be measured for the specific set of particles [62]. In addition to experimentally quantifying model parameters, the development of realistic numerical boundary conditions should be a focus. Developing these boundary conditions is a significant future research challenge, but recent work has made excellent progress towards this goal [48, 49]. The observation in the 30° silo that the flow regime changes from mass to rat-holing when the boundary condition changed exemplifies the necessity of accurate boundary conditions and may indicate something more complex than a simple slip condition is needed. Finally, in recent times it has

been shown that defining an effective granular viscosity using the  $\mu(I)$  friction model with an incompressible flow assumption can be mathematically ill-posed depending on the choice of parameters [63]. Adding the effect of compressibility seems to alleviate this issue [50, 64]. Although we did not note any issues in our model for our choice of parameters, this fact serves as an additional motivation to transition to a compressible flow model of granular drainage from a silo.

The authors acknowledge the Manawatu Microscopy Imaging Centre (MMIC) at Massey University for producing the SEM images of the poppy seeds in Figure 1. L.F. also acknowledges funding from the Royal Society of New Zealand (contracts RFT-MAU1501-PD and MAU1712). Finally, we acknowledge the help of Maral Mehdizad and Alex Cliff to quantify the mass flow rates in the system.

- 
- [1] Bruno Andreotti, Yoël Forterre, and Olivier Pouliquen, *Granular media: between fluid and solid* (Cambridge University Press, 2013).
- [2] Ronald Midgley Nedderman, *Statics and kinematics of granular materials* (Cambridge University Press, 2005).
- [3] K Kesava Rao, Prabhu R Nott, and S Sundaresan, *An introduction to granular flow*, Vol. 10 (Cambridge University Press New York, 2008).
- [4] M Combarros Garcia, HJ Feise, S Strege, and A Kwade, “Segregation in heaps and silos: Comparison between experiment, simulation and continuum model,” *Powder Technology* **293**, 26–36 (2016).
- [5] Thomas Weinhart, Carlos Labra, Stefan Ludwig, and Jin Y Ooi, “Influence of coarse-graining parameters on the analysis of dem simulations of silo flow,” *Powder technology* **293**, 138–148 (2016).
- [6] Davide Bertuola, Silvia Volpato, Paolo Canu, and Andrea C Santomaso, “Prediction of segregation in funnel and mass flow discharge,” *Chemical Engineering Science* **150**, 16–25 (2016).
- [7] L Staron, P-Y Lagrée, and S Popinet, “Continuum simulation of the discharge of the granular silo,” *The European Physical Journal E* **37**, 5 (2014).
- [8] Lydie Staron, P-Y Lagrée, and Stéphane Popinet, “The granular silo as a continuum plastic flow: The hour-glass vs the clepsydra,” *Physics of Fluids* **24**, 103301 (2012).
- [9] Silvia Volpato, Riccardo Artoni, and Andrea C Santomaso, “Numerical study on the behavior of funnel flow silos with and without inserts through a continuum hydrodynamic approach,” *Chemical Engineering Research and Design* **92**, 256–263 (2014).
- [10] Yin Wang and Jin Y Ooi, “A study of granular flow in a conical hopper discharge using discrete and continuum approach,” *Procedia engineering* **102**, 765–772 (2015).
- [11] Sachith Dunatunga and Ken Kamrin, “Continuum modelling and simulation of granular flows through their many phases,” *Journal of Fluid Mechanics* **779**, 483–513 (2015).
- [12] Luke A Fullard, Clive E Davies, and Graeme C Wake, “Modelling powder mixing in mass flow discharge: A kinematic approach,” *Advanced Powder Technology* **24**, 499–506 (2013).

- [13] Luke Fullard, Eric Breard, Clive Davies, Pierre-Yves Lagr  e, St  phane Popinet, and Gert Lube, "Testing the  $\mu$  (i) granular rheology against experimental silo data," in *EPJ Web of Conferences*, Vol. 140 (EDP Sciences, 2017) p. 11002.
- [14] Y Zhou, P-Y Lagr  e, S Popinet, P Ruyer, and Pascale Aussillous, "Experiments on, and discrete and continuum simulations of, the discharge of granular media from silos with a lateral orifice," *Journal of Fluid Mechanics* **829**, 459–485 (2017).
- [15] LA Fullard, CE Davies, AC Neather, ECP Breard, AJR Godfrey, and G Lube, "Testing steady and transient velocity scalings in a silo," *Advanced Powder Technology* **29**, 310–318 (2018).
- [16] LA Fullard, CE Davies, G Lube, AC Neather, ECP Breard, and BJ Shepherd, "The transient dynamics of dilation waves in granular phase transitions during silo discharge," *Granular Matter* **19**, 6 (2017).
- [17] Jaehyuk Choi, Arshad Kudrolli, and Martin Z Bazant, "Velocity profile of granular flows in side silos and hoppers," *Journal of Physics: Condensed Matter* **17**, S2533 (2005).
- [18] A Janda, Iker Zuriguel, A Garcimart  n, Luis A Pagnaloni, and Diego Maza, "Jamming and critical outlet size in the discharge of a two-dimensional silo," *EPL (Europhysics Letters)* **84**, 44002 (2008).
- [19] I Sielamowicz, S Blonski, and TA Kowalewski, "Optical technique dpiv in measurements of granular material flows, part 1 of 3 plane hoppers," *Chemical Engineering Science* **60**, 589–598 (2005).
- [20] K Endo, K Anki Reddy, and H Katsuragi, "Obstacle-shape effect in a two-dimensional granular silo flow field," *Physical Review Fluids* **2**, 094302 (2017).
- [21] Selam Waktola, Andre Bieberle, Frank Barthel, Martina Bieberle, Uwe Hampel, Krzysztof Grudzie  , and Laurent Babout, "A new data-processing approach to study particle motion using ultrafast x-ray tomography scanner: case study of gravitational mass flow," *Experiments in Fluids* **59**, 69 (2018).
- [22] Krzysztof Grudzien, Maciej Niedostatkiewicz, Jerome Adrien, Eric Maire, and Laurent Babout, "Analysis of the bulk solid flow during gravitational silo emptying using x-ray and computed tomography," *Powder technology* **224**, 196–208 (2012).
- [23] H-Y Xie and K Shinohara, "Measurement of solids velocity in a conical hopper by mass tracer particles," *Chemical engineering science* **54**, 455–459 (1999).
- [24] PA Langston, MS Nikitidis, U T  z  n, DM Heyes, and NM Spyrou, "Microstructural simulation and imaging of granular flows in two-and three-dimensional hoppers," *Powder Technology* **94**, 59–72 (1997).
- [25] MS Nikitidis, U T  z  n, and NM Spyrou, "Determination of phase velocities in multi-phase flows in hoppers using dual photon gamma-ray tomography," *Chemical Engineering Communications* **175**, 3–24 (1999).
- [26] Michail S Nikitidis, Ugur T  z  n, and Nicholas M Spyrou, "Tomographic measurements of granular flows in gases and in liquids," *KONA Powder and Particle Journal* **12**, 53–67 (1994).
- [27] Ralf Stannarius, "Magnetic resonance imaging of granular materials," *Review of Scientific Instruments* **88**, 051806 (2017).
- [28] Alexander Penn, Takuya Tsuji, David O Brunner, Christopher M Boyce, Klaas P Pruessmann, and Christoph R M  ller, "Real-time probing of granular dynamics with magnetic resonance," *Science Advances* **3**, e1701879 (2017).
- [29] Christopher M Boyce, Alexander Penn, Klaas P Pr  ssmann, and Christoph R  diger M  ller, "Magnetic resonance imaging of gas-solid fluidization with liquid bridging," *AIChE Journal* (2017).
- [30] CM Boyce, NP Rice, A Ozel, JF Davidson, Andrew John Sederman, Lynn Faith Gladden, S Sundaresan, John Stephen Dennis, and DJ Holland, "Magnetic resonance characterization of coupled gas and particle dynamics in a bubbling fluidized bed," *Physical Review Fluids* **1**, 074201 (2016).
- [31] Hilary T Fabich, Andrew J Sederman, and Daniel J Holland, "Development of ultrafast x-ray imaging for granular systems," *Journal of Magnetic Resonance* **273**, 113–123 (2016).
- [32] CM Boyce, A Ozel, NP Rice, GJ Rubinstein, DJ Holland, and S Sundaresan, "Effective particle diameters for simulating fluidization of non-spherical particles: Cfd-dem models vs. mri measurements," *AIChE Journal* **63**, 2555–2568 (2017).
- [33] Hilary T Fabich, Andrew J Sederman, and Daniel J Holland, "Study of bubble dynamics in gas-solid fluidized beds using ultrashort echo

- time (ute) magnetic resonance imaging (mri),” *Chemical Engineering Science* **172**, 476–486 (2017).
- [34] HT Fabich, TI Brox, D Clarke, JD Seymour, SL Codd, P Galvosas, J Brown, AJ Sederman, and DJ Holland, “Measurements of the velocity distribution for granular flow in a couette cell,” *Physical Review E* **98**, 062901 (2018).
- [35] Toshihiro Kawaguchi, “Mri measurement of granular flows and fluid-particle flows,” *Advanced Powder Technology* **21**, 235–241 (2010).
- [36] Michael Gentzler and Gabriel I Tardos, “Measurement of velocity and density profiles in discharging conical hoppers by nmr imaging,” *Chemical Engineering Science* **64**, 4463–4469 (2009).
- [37] ZH Gu, PC Arnold, and AG McLean, “Prediction of the flowrate of bulk solids from mass flow bins with conical hoppers,” *Powder technology* **72**, 157–166 (1992).
- [38] Pierre Jop, Yoël Forterre, and Olivier Pouliquen, “A constitutive law for dense granular flows,” *Nature* **441**, 727 (2006).
- [39] P-Y Lagrée, Lydie Staron, and Stéphane Popinet, “The granular column collapse as a continuum: validity of a two-dimensional navier–stokes model with a  $\mu$  (i)-rheology,” *Journal of Fluid Mechanics* **686**, 378–408 (2011).
- [40] Przemyslaw B Kowalczyk and Jan Drzymala, “Physical meaning of the sauter mean diameter of spherical particulate matter,” *Particulate Science and Technology* **34**, 645–647 (2016).
- [41] Kiwing To, “Jamming transition in two-dimensional hoppers and silos,” *Physical Review E* **71**, 060301 (2005).
- [42] Nan Gui, Xingtuan Yang, Jiyuan Tu, and Shengyao Jiang, “Effects of rocking frequency and amplitude on particle discharge in rocking bed: A dem study,” *Powder technology* **292**, 31–45 (2016).
- [43] Arnold McLean, “The use of standpipes for increasing limiting gravitational flowrate from mass flow bins,” *KONA Powder and Particle Journal* **11**, 139–145 (1993).
- [44] C Mankoc, A Janda, Roberto Arevalo, JM Pastor, Iker Zuriguel, A Garcimartín, and Diego Maza, “The flow rate of granular materials through an orifice,” *Granular Matter* **9**, 407–414 (2007).
- [45] W Ar Beverloo, Hendrik Antonie Leniger, and J Van de Velde, “The flow of granular solids through orifices,” *Chemical engineering science* **15**, 260–269 (1961).
- [46] Paul T. Callaghan, *Translational Dynamics and Magnetic Resonance*, 1st ed. (Oxford University Press, Oxford, 2011).
- [47] Stéphane Popinet, “Gerris: a tree-based adaptive solver for the incompressible euler equations in complex geometries,” *Journal of Computational Physics* **190**, 572–600 (2003).
- [48] Riccardo Artoni, Andrea C Santomaso, Massimiliano Go, and Paolo Canu, “Scaling laws for the slip velocity in dense granular flows,” *Physical review letters* **108**, 238002 (2012).
- [49] Riccardo Artoni and Andrea Santomaso, “Effective wall slip in chutes and channels: experiments and discrete element simulations,” *Granular Matter* **16**, 377–382 (2014).
- [50] Thomas Barker, DG Schaeffer, Michael Shearer, and JMNT Gray, “Well-posed continuum equations for granular flow with compressibility and  $\mu$  (i)-rheology,” *Proc. R. Soc. A* **473**, 20160846 (2017).
- [51] Luke Fullard and Clive Davies, “Minimising the spread of residence-time distribution for flat and heaped powders in a wedge-shaped planar hopper,” *Particuology* **30**, 102–110 (2017).
- [52] Kenneth E Fickie, Reza Mehrabi, and Roy Jackson, “Density variations in a granular material flowing from a wedge-shaped hopper,” *AIChE journal* **35**, 853–855 (1989).
- [53] RL Brown, “Minimum energy theorem for flow of dry granules through apertures,” *Nature* **191**, 458 (1961).
- [54] Mebirika Benyammine, Pascale Aussillous, and Blanche Dalloz-Dubrujeaud, “Discharge flow of a granular media from a silo: effect of the packing fraction and of the hopper angle,” in *EPJ Web of Conferences*, Vol. 140 (EDP Sciences, 2017) p. 03043.
- [55] David L Henann and Ken Kamrin, “A predictive, size-dependent continuum model for dense granular flows,” *Proceedings of the National Academy of Sciences* **110**, 6730–6735 (2013).
- [56] GDR MiDi, “On dense granular flows,” *The European Physical Journal E* **14**, 341–365 (2004).
- [57] Pierre Jop, Yoël Forterre, and Olivier Pouliquen, “Crucial role of sidewalls in granular surface flows: consequences for the rheology,” *Journal of Fluid Mechanics* **541**, 167–192 (2005).
- [58] Emilien Azéma, Nicolas Estrada, Itthichai Preechawuttipong, Jean-Yves Delenne, and Farhang Radjai, “Systematic description of the

- effect of particle shape on the strength properties of granular media,” in *EPJ Web of Conferences*, Vol. 140 (EDP Sciences, 2017) p. 06026.
- [59] Shiwei Zhao and Xiaowen Zhou, “Effects of particle asphericity on the macro-and micro-mechanical behaviors of granular assemblies,” *Granular Matter* **19**, 38 (2017).
- [60] Tamás Börzsönyi, Ellák Somfai, Balázs Szabó, Sandra Wegner, Ahmed Ashour, and Ralf Stannarius, “Elongated grains in a hopper,” in *EPJ Web of Conferences*, Vol. 140 (EDP Sciences, 2017) p. 06017.
- [61] Ezequiel Goldberg, C Manuel Carlevaro, and Luis A Pugnaloni, “Effect of grain shape on the jamming of two-dimensional silos,” in *EPJ Web of Conferences*, Vol. 140 (EDP Sciences, 2017) p. 06009.
- [62] Abdoulaye Fall, Guillaume Ovarlez, David Hautemayou, Cédric Mézière, J-N Roux, and François Chevoir, “Dry granular flows: Rheological measurements of the  $\mu$  (i)-rheology,” *Journal of rheology* **59**, 1065–1080 (2015).
- [63] T Barker, DG Schaeffer, P Bohorquez, and JMNT Gray, “Well-posed and ill-posed behaviour of the  $\mu(i)$ -rheology for granular flow,” *Journal of Fluid Mechanics* **779**, 794–818 (2015).
- [64] Joris Heyman, R Delannay, H Tabuteau, and A Valance, “Compressibility regularizes the  $\mu(i)$ -rheology for dense granular flows,” *Journal of Fluid Mechanics* **830**, 553–568 (2017).